

See discussions, stats, and author profiles for this publication at: <https://www.researchgate.net/publication/244403316>

Molecular Dynamics Simulations of Intercalated Poly(ϵ -Caprolactone)Montmorillonite Clay Nanocomposites

ARTICLE in THE JOURNAL OF PHYSICAL CHEMISTRY B · JULY 2004

Impact Factor: 3.3 · DOI: 10.1021/jp0493069

CITATIONS

39

READS

52

4 AUTHORS, INCLUDING:



Fabrice Gardebien

Université des Antilles et de la Guyane

21 PUBLICATIONS 351 CITATIONS

SEE PROFILE



Anouk Gaudel Siri

Aix-Marseille Université

31 PUBLICATIONS 329 CITATIONS

SEE PROFILE



Roberto Lazzaroni

Université de Mons

400 PUBLICATIONS 9,352 CITATIONS

SEE PROFILE

Molecular Dynamics Simulations of Intercalated Poly(ϵ -Caprolactone)-Montmorillonite Clay Nanocomposites

Fabrice Gardebien,^{*,†} Anouk Gaudel-Siri,[‡] Jean-Luc Brédas,^{†,§} and Roberto Lazzaroni[†]

Service de Chimie des Matériaux Nouveaux, Université de Mons-Hainaut, 20 Place du Parc, B-7000 Mons, Belgium, Laboratoire Réso - UMR 6178, Université Paul Cézanne, Faculté St Jérôme, Av. Esc. Normandie-Niemen, 13397 Marseille Cedex 20, France, and School of Chemistry and Biochemistry, Georgia Institute of Technology, Atlanta, Georgia 30332-0400

Received: February 16, 2004; In Final Form: May 11, 2004

The structure and energetics of poly(ϵ -caprolactone), PCL, chains confined between two platelets of organo-modified montmorillonite clay, are investigated using molecular dynamics techniques. The amount of PCL in the clay gallery has been systematically varied to assess the influence of the interlayer density on the molecular organization. The structural characteristics are examined in terms of interlayer density profiles, radial distribution functions, and dihedral angle distributions. The results show that the interlayer phase organizes into four layers, along with an enhancement of the proportion of extended zigzag chain conformations, with respect to the amorphous polymer bulk. Calculations of the interaction energies between the various subsystems (the PCL chains, the surfactant molecules, and the clay surfaces) clearly show the formation of polar as well as apolar interactions between PCL and the clay surfaces, which can significantly contribute to the polymer intercalation (in addition to the polymer–surfactant interactions).

1. Introduction

A promising area in polymer technology is the development of polymer–clay nanocomposites (PNCs). In this new class of materials, layered clay particles are distributed within a polymer matrix. Depending on the PNC constituents or the preparation route, three structural arrangements have been observed, termed: (a) intercalated, where the polymer chains are organized within the interlayer spaces formed by parallel arrangements of the clay layers, (b) exfoliated or delaminated, in which the individual clay layers are evenly dispersed in the polymer matrix, and (c) composites, where the polymer and the clay particles are immiscible and consist of stacks of clay layers spread inside the polymer matrix. For clay contents as low as 2 wt %, improvements in mechanical, thermal, or barrier properties have been evidenced for the PNCs with respect to conventional polymer microcomposites, with larger enhancement in properties achieved for exfoliated systems (for a review, see ref 1). Among the clays that are commonly employed in PNCs, the most prominent are smectite-type clays such as montmorillonite (mmt), whose crystal lattice consists of negatively charged aluminosilicate layers. It should be stressed that, in order to increase the miscibility between the polymer matrix (often hydrophobic) and the pristine clay (highly hydrophilic), many experiments are conducted using clays in which the natural metal cations that balance the charge deficiency have been substituted by organophilic cations such as alkylammoniums.^{2–7}

Prior to recent theoretical efforts devoted to PNCs, the structural arrangement and dynamical behavior of polymer chains confined between neutral solid planes had been studied using molecular simulations techniques.^{8–12} For the confined

polymer, the main structural observations are: (i) near the planes, the polymer chains are flattened and the density of chain ends is enhanced, regardless of the strength of the interaction between the polymer and the surface, and (ii) segments in the center of the polymer chains end up near the planes in the case of strong polymer–surface interactions (with an interfacial density higher than that of the polymer bulk value) and mainly away from the planes in the case of moderate interactions. Strong polymer–surface interactions also lower the mobility of the interfacial polymer segments in all directions.¹¹ As for the PNCs, mean-field approaches have provided a general framework for their description.^{13–16} Vaia et al. have developed a mean-field model to describe polymer melt intercalation in organically modified layered silicates;^{13,14} these authors discussed the entropic and enthalpic factors that favor intercalation and exfoliation. Balazs et al. derived useful criteria for facile intercalation: the polymer must contain a fragment that is highly attracted to the surface but also a longer fragment that is not attracted to the sheets.¹⁶ Lee et al.^{17,18} have investigated the intercalation process by simulating the flow of polymer chains represented by connected beads into a narrow slit. An important conclusion of these works is that increasing the polymer–surface interaction favors the intercalation; however, their results also indicate a decreased propensity for intercalation when polymer–silicate affinity is too high (for results compared within the same period of simulation time). The effects of both the polymer molecular weight and the polymer–surface interactions on the kinetics of the intercalation process have also been investigated by the same authors.¹⁹ For PNCs based on polystyrene^{20,21} and poly(ethylene oxide) (PEO),^{22–24} combined molecular dynamics (MD) and NMR studies showed important inhomogeneities in their dynamical behavior across the clay gallery and over a wide range of temperature;²³ confined PEO appears to be more disordered than its bulk amorphous counterpart.^{22–24} For PNCs based on nylon-6, systematic studies of the influence of the size

* To whom correspondence may be addressed. E-mail: Fabrice@averell.umh.ac.be. Fax: ++32-65-37-38-61.

[†] Université de Mons-Hainaut.

[‡] Université Paul Cézanne.

[§] Georgia Institute of Technology.

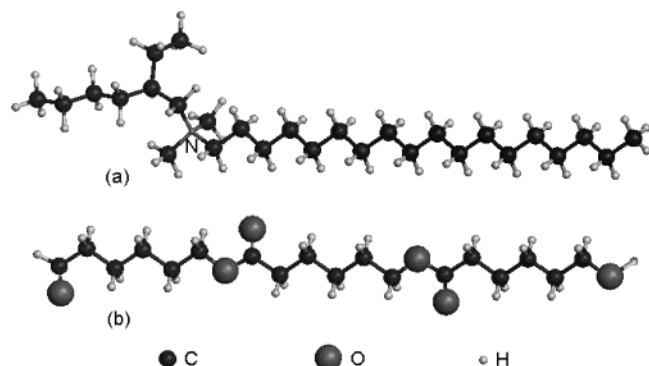


Figure 1. Molecular structures of (a) the dimethyl 2-ethylhexyl *n*-octadecylammonium ion that corresponds to the surfactant used throughout this study and (b) a PCL chain of 3 monomer units (3-mer).

of the organic modifier have established that the pristine mmt clay (with its natural metal cations) is preferred for a maximum interfacial strength with the polymer matrix.^{25,26} Besides these works on polymer–silicate systems, hydrated pristine silicates have been the topics of extensive studies in the literature (see, for example, ref 27 and the references therein).

The biodegradable and biocompatible polymer poly(ϵ -caprolactone) (PCL), a linear aliphatic polyester, has shown a great ability to form intercalated PNCs with mmt clays rendered organophilic by cation exchange. The intrinsic interesting properties of this polymer, combined with those potentially gained by PNC formation, have prompted joint experimental and theoretical studies of PCL-based nanocomposites.^{28–32} In this work, we present the results of MD simulations carried out on model systems for intercalated PCL nanocomposites. In these models, short PCL chains are confined between two parallel platelets of montmorillonite whose metal ions have all been replaced by dimethyl 2-ethylhexyl *n*-octadecylammoniums. Our goal is to probe the structural arrangements of the intercalated PCL chains using atomistic simulations that allow a close look at the material at the nanoscopic level and help in understanding the intimate organization between the three components of the systems (PCL, mmt, and surfactants). The interactions between the components were also examined. The results provide some insights into the factors that favor intercalation of the PCL. MD simulations were also conducted for amorphous samples of PCL, and their results are used throughout the analyses as a basis for comparison. This study of the intercalated system is our first contribution to the modeling of PNCs based on PCL; a forthcoming paper will present the results of simulations for exfoliated PCL–mmt models.

The paper is organized as follows: the Methodology section describes successively the selection procedure of the force field, the models used to treat our PNC system, the details of the MD simulations, and the procedures followed to derive initial configurations. The results of the simulations are presented and discussed in section 3. A final discussion is provided in the Conclusion.

2. Methodology

2.1. Force-Field Selection Procedure. To select an appropriate force field for the description of nanocomposite systems based on PCL chains (Figure 1) and organo-modified montmorillonite, a preliminary study was conducted to obtain an appropriate force field for the description of the polymer. This

is important since a correct description of the interactions between the polymer chains is essential for obtaining details of their structural properties at interfaces.³³ Three force fields were considered: the universal force field (UFF),³⁴ the Dreiding force field,³⁵ and a hybrid force field hereafter noted DT. The DT force field uses the Dreiding force-field parameters for the bond, angle, torsion, and inversion parameters and the Tripos parameters³⁶ for the nonbonded van der Waals parameters. In that force field, the H-bond term present in the Dreiding original force field has been turned off since no significant H bonds are expected in the polymer system and in our nanocomposite systems. For the electrostatic interactions, the charges are taken in all cases from an electrostatic potential calculation carried out on a smaller oligomer species (vide infra). The rationale behind the choice of using the Tripos nonbonded parameters comes from a previous comparative study of the van der Waals parameters of the three force fields (UFF, Dreiding, and Tripos) with *ab initio* MP2 calculations for an organic cluster adsorbed on a small aluminosilicate structure that mimics the clay surface.³⁷ A slightly better agreement with the results at the MP2 level were obtained for the Tripos van der Waals parameters.

MD simulations of amorphous PCL were considered for the three force fields in the NPT ensemble at 300 K. The simulation cells comprised 3 chains of 48 monomer units each. The amorphous polymer builder module and the OFF module available in the Cerius² modeling environment³⁸ were used for the generation of the amorphous configurations and for the molecular mechanics and dynamics calculations, respectively. Three configurations were generated; for each one, a NVT simulation using UFF at 300 K during 50 ps was first performed. For each of the resulting cells, two successive annealing cycles in the NVT ensemble were considered with the following temperatures and durations for both cycles: heating at 1000 K for 30 ps and then cooling at 700 K for 25 ps and at 300 K during 15 ps. Using the configurations obtained, NPT dynamics at 300 K followed during 100 ps to derive the final density value for the simulated amorphous PCL. The cell whose density comes closest to the experimental density was selected for runs according to the above-described procedure using the Dreiding and DT force fields: 50 ps of NVT dynamics at 300 K, followed by the two successive annealing cycles and ultimately by 100 ps of NPT dynamics. The densities obtained for the amorphous PCL are 1.04 and 1.01 g·cm^{−3} for UFF and the DT force field, respectively. The much lower value reached for simulations using the Dreiding force field, 0.93 g·cm^{−3}, suggests an inadequacy between the van der Waals parameters of this force field and the calculated set of atomic charges for the chains. Since the results obtained with UFF better match the experimental density value of 1.09 g·cm^{−3} for amorphous PCL, this force field was selected for the simulations of our PNC.

2.2. Models for the Polymer Nanocomposite. For systems that correspond to chains confined between adsorbing surfaces, it has been argued that efficient packing of the chains in the interlayer space may favor a higher interlayer density.³⁹ Since no information about the efficiency with which the chains are packed inside the gallery is available, the *a priori* choice of an interlayer density value for the organic phase (which amounts to determining the quantity of PCL, since the number of organophilic cations is known and equals the total charge borne by a clay platelet, that is, 9 in our simulation cell) is delicate. Our approach was to extend our study over a narrow range of plausible interlayer organic densities which were derived using the procedure described below. To calculate the interlayer

density, only the volume available to the organic molecules was considered. This volume is estimated as $L_x L_y (L_z - 2d_z)$, where L_x and L_y are the lengths of the simulation box in the x and y directions and L_z is the distance between two facing planes of basal oxygen atoms in the z direction. The distance d_z is the minimum distance at which an organic molecule can approach the aluminosilicate surface, and it is taken as half the van der Waals radius of the basal oxygen atoms. On the basis of experimental observations for the PCL polymer, three initial interlayer densities, i.e., three amounts of PCL to be inserted inside the gallery, were considered. Experimental measurements for PCL have provided density values for the amorphous and crystalline parts at 300 K of 1.09 and 1.21 g·cm⁻³, respectively.⁴⁰ Accordingly, based on the assumption that the density of the organic phase in the gallery is the same as the density of the bulk polymer, the following two systems were considered: the first with 3 chains of 8 monomer units each (hereafter denoted system II) and the second with 2 chains of 14 monomers (system III), which correspond to a density of 1.11 and 1.19 g·cm⁻³ for the organic phase in the interlayer space, respectively. Additionally, since our force field slightly underestimates the experimental density for the amorphous polymer (see section 2.1), we chose the following lowest limit value, 1.03 g·cm⁻³, for the interlayer organic phase; this corresponds to a system made up of 2 chains of 10 monomer units (system I). As mentioned earlier, in addition to the polymer chains, the gallery of the three systems contains nine surfactant molecules.

2.3. Simulation Cell. Montmorillonite is an aluminosilicate made up of one aluminate octahedral sheet sandwiched by two silicate tetrahedral sheets. Isomorphous substitution of metal ions in the crystal lattice by cations of lower charge causes a net permanent negative charge which is balanced by cations in the interlayer space. The model chosen for the montmorillonite clay has been taken from the work of Skipper et al.⁴¹ The unit layer considered in this study with x and y dimensions of 31.7 Å by 18.3 Å bears a negative charge of 9 e, which results from the substitutions of Si atoms by Al atoms and Al atoms in octahedral positions by Mg atoms.

The third dimension of the simulation box, which corresponds to the interlayer distance, was chosen to match the experimental value determined by X-ray diffraction experiments for our PNC, 26.8 Å.^{30,31} The positive charges in the interlayer space were borne by 9 dimethyl 2-ethylhexyl *n*-octadecylammonium ions (Figure 1); this surfactant corresponds to the main organic modifier in the organically modified commercial montmorillonite Cloisite 25A.

2.4. Simulation Details. The calculations were performed within the Cerius² modeling environment.³⁸ The UFF³⁴ was considered for all simulations except where otherwise stated. Throughout all simulations, the positions of the atoms of the clay were fixed. These restraints on the clay atomic positions are commonly used and have proven to be pertinent since reliable results can be obtained with reasonable computational efforts.^{42–44} For the treatment of the electrostatic interactions, the Ewald summation method was used.⁴⁵ The charges on the atoms (see appendix) of the individual surfactant molecules and polymer chains (of lengths up to 8 units) were obtained by fits to the electrostatic potentials derived from ab initio HF/6-31G-(d) calculations (CHELPG method⁴⁶ as implemented in the program system Gaussian 98⁴⁷). This approach is known to provide a more realistic description of the charge distribution, compared to the more commonly used charge-equilibration method⁴⁸ or Mulliken population analysis. For the longer polymer chains (10-, 14-, and 48-mer), the charges were

obtained with the same technique but performed on subunits. For example, the charges for the 48-mer were derived from a calculation made on an octamer. The 48-mer was then constructed as six octamers with the atomic charges at their junctions modified so as to match those of an ester function in the inner part of an octamer. The charges on all atoms were kept fixed during the simulations. For the van der Waals interactions, the Lennard-Jones potential was driven smoothly to zero for distances between 8 and 9 Å. Three-dimensional periodic boundary conditions were imposed in order to avoid boundary artifacts. All simulations were performed in the NVT ensemble and used a coupling to a Nosé–Hoover thermostat^{49–51} to maintain the temperature.

2.5. Procedure for Generating the Initial Configurations.

Two different procedures were followed for generating configurations for the MD simulations of nanocomposite systems I, II, and III. A first step common to both procedures was to find initial guess configurations for a surfactant or for a polymer chain as starting configurations in the interlayer space. These initial configurations were obtained by using the RIS Metropolis Monte Carlo (RMMC) method.⁵² The selected configurations had to satisfy two criteria: to have the lowest possible potential energy and a shape that fit in the simulation box.

Once individual configurations were generated for the molecules in the gallery, the first procedure consisted in increasing the interlayer distance by small steps of 1 Å from the initial value 26.8 Å up to 35 Å for the two systems of lowest densities I and II and up to 40 Å for system III, which corresponds to the highest interlayer density and to the longest PCL chains. While increasing the interlayer space, short MD runs of 8 ps were performed for each intermediate interlayer distance, at a temperature of 2500 K to speed up the conformational sampling. At the maximum interlayer space, the dynamics run was extended to 15 ps before decreasing back the interlayer distance toward its initial value by steps of 0.5 Å, again with short runs of 10 ps at 2500 K. When the interlayer distance of 26.8 Å is recovered, an annealing procedure is performed by cooling to 300 K over a 85-ps period.

The second procedure to derive initial configurations for systems I, II, and III was the following: after insertion in the gallery of the configurations generated for the individual organic molecules by using RMMC, we ran MD calculations using a force field properly modified to sample efficiently the conformation space of the organic phase. Since the UFF force field uses a set of functional forms to generate its parameters, we selected instead the Dreiding force field to impose relevant modifications of its bonded and nonbonded parameters. The Dreiding force field was modified as follows: the torsional barrier height k_{CC} around all CC bonds was set to zero. Additionally, the van der Waals and electrostatic 1–4 interactions were excluded from the total potential energy. Finally, in the 12-6 Lennard-Jones expression, the ϵ_H parameter was scaled down to favor configurational changes by decreasing the intermolecular interactions. For each system, an explorative MD calculation was run over 200 ps at 300 K. The following step was to extract only a few pertinent configurations from the generated set. This was done according to two criteria related to the potential energy: typically, three configurations were extracted for each of the three systems on the basis of both the lowest nonbonded energy and the lowest possible total torsional energy. The bond and angle energetic contributions were discarded from the selection criteria for two reasons. First, their large contributions to the potential energy may bias the selection toward, for example, configurations corresponding to high

nonbonded energy terms and accidentally low bond and angle potential terms. Second, the successive values of the bond and angle energy contributions cannot be directly related to the configuration changes of the whole interlayer system. Once some guess configurations have been generated, the true interatomic potential was restored. Using UFF, a simulated annealing cycle was then carried out for each selected configuration in order to find the lowest-energy configuration when all interatomic interactions are considered.

By use of the configurations resulting from these two procedures, MD simulations at 300 K were then run for 250 ps. Afterward, for each series associated to systems I, II, and III, the structure corresponding to the lowest potential energy was selected for the analyses. Note that the structure of lowest potential energy was derived from 250-ps simulations following the second procedure for the system of lowest density (system I) and following the first procedure for systems with the highest densities (systems II and III). For the analyses, we ensured that the structures were equilibrated by monitoring the potential energy, temperature, and the nonbond energy variations. The period of time required to achieve equilibration was typically in the range of 50–150 ps. The energy calculations of the intermolecular interactions are made for geometries minimized until a root-mean-square convergence ≤ 0.001 kcal/mol/Å in the energy gradient was achieved.

3. Results and Discussion

3.1. Description of the Molecular Organization. Figure 2 shows the final configurations obtained for the three PNC model systems I, II, and III. Apart from its ester function, the caprolactone monomer unit contains five successive methylene groups. One would therefore expect the corresponding polymer to prefer the most hydrophobic region of the interlayer gallery, that is, the central region of the slit. However, our simulations indicate that the polar ester functions show a tendency to interact with the clay surface. An explanation for this polymer–clay interaction resides in long-range electrostatic interactions between, on one hand, the ester function (polar group) and the polarized adjacent methylene group and, on the other hand, the clay layers; this seems to be the main force driving the polymer chains to the surface for subsequent electrostatic and van der Waals interactions with the clay atoms. The polarization of the methylene group adjacent to the ester function is due to hyperconjugation between one of its σ_{CH} molecular orbitals with the delocalized π system of the ester function, thus partly decreasing the electronic density on the corresponding methylene group. The calculated charge on the corresponding carbon (as obtained by the CHELPG method) is about $+0.45$ e, and the global charge for the corresponding CH_2 group is around $+0.40$ e (for comparison, the global charge on the following CH_2 neighbor decreases sharply to 0). When the PCL chains are still far from the clay surfaces, its positively charged methylenes appear to be the most effective polymer sites for bringing the polymer chains toward the negatively charged layers. Indeed, both oxygen atoms of the ester functions bear large negative charges (~ -0.6 e), and at long distance, they do not feel any attraction to the surface due to the negative charges in the clay layers. This result points out the importance of reliable charge determinations (such as those derived from electrostatic potentials using *ab initio* methods) and their incidence on the geometry adopted by the interlayer system. As is also suggested by mean-field models for the free energy of the polymer melt and closely spaced sheets,¹⁶ this PCL–mmt interaction could explain (at least partly) the intercalation of the polymer into

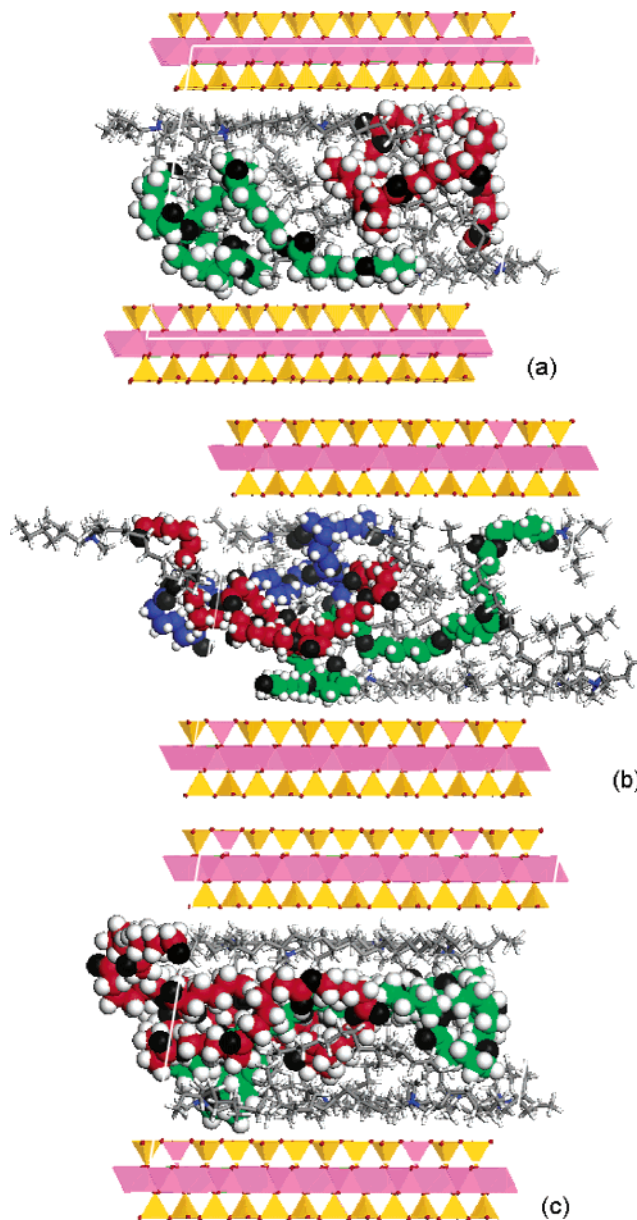


Figure 2. Snapshots of the simulations of (a) PNC system I, (b) PNC system II, and (c) PNC system III obtained after 250 ps of MD calculations. The clay layers are represented by one octahedral sheet sandwiched between two tetrahedral sheets. In the gallery, the surfactants are represented with sticks and the PCL chains with spheres; the carbon atoms are in green, red, and blue, the oxygen atoms in black, and the hydrogen atoms in white.

the mmt gallery, as observed experimentally, and also contributes to the miscibility between PCL and the clay.

When the polymer segments migrate toward the surface, some of the surfactant tails leave portions of the surface and move to the center of the slit (which is mostly hydrophobic) to interact with the rest of the PCL chains. In contrast to the hydrophobic tails, the charged heads of the surfactants remain, as expected, stuck to the surface. Hence, it appears that both types of chains (polymer and surfactant) show a dual behavior distributed over the center (mainly hydrophobic region) and onto the surfaces (hydrophilic region) inside the gallery. Structural and energetic analyses are provided hereafter in order to get some insight into the organization adopted by the organic phase in the interlayer space.

Figure 3 shows the contributions of the backbone atoms (carbon and oxygen) of the surfactants and the PCL chains to

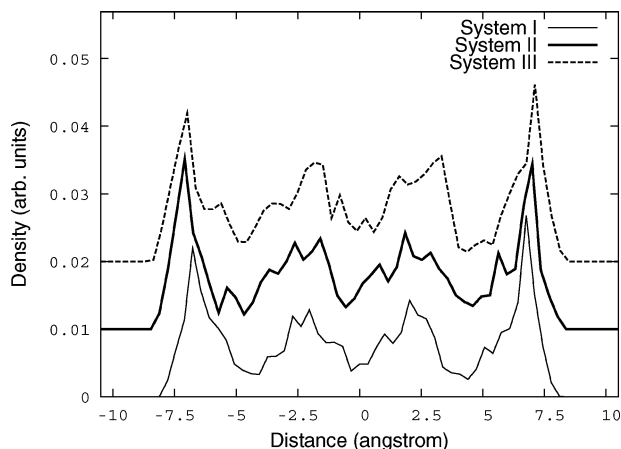


Figure 3. Density profiles for the backbone atoms of the surfactants and PCL chains in the direction normal to the clay layers, reported for the PNC systems I, II, and III. The positions of the two planes of basal oxygen atoms are at ± 10.5 Å. For clarity, the profiles for systems II and III have been shifted by 0.01 and 0.02 along the y axis, respectively.

the interlayer atomic density profile, in the direction normal to the clay platelets, for the three systems. In all three cases, one can see that the system organizes into four layers inside the gallery. This layering effect is well-known for confined liquids⁵³ and arises from solvation forces. However, the profile obtained for confined polymers cannot adopt the smooth aspect observed for confined liquids (at least when considering a simulation box of reasonable size) since the atoms have the additional constraint of being connected along chains that run across many adjacent organic layers. For a given system (I, II, or III), it is clear from Figure 3 that the four peaks have rather different heights and widths depending on their location inside the gallery. The two peaks closer to the clay layers turn out to be the highest; their height is actually related to the force of the interactions existing between the clay surface and the adsorbed chains; the stronger these interactions, the higher the associated peaks.¹¹ For both systems I and II, higher and sharper peaks are observed for the two layers closer to the clay surface, whereas broader and smaller peaks are obtained for the two innermost layers. For system III, the peaks associated to the two directly adsorbed organic layers are still sharp and high; however, the outlines of the two innermost layers are less clear-cut: the two central peaks are broad, and the valley at the center is not very deep (for this system, one might even discern the presence of a small fifth peak in the center of the gallery). The two central layers for this system are actually more spread than their counterparts in the lower density systems. The spreading of these two peaks can be interpreted as an indication that the interlayer phase has reached its highest density limit for this particular interlayer distance, as suggested by Hackett et al. in their work on organically modified layered silicates.⁵⁴ This is how the system tries to accommodate to the excess interlayer density. Since system III seems to correspond to the highest interlayer density limit, it is therefore reasonable to think that the three model systems we have chosen bracket a realistic amount of PCL present in the slit for the PNC model studied here.

It should also be noticed that, initially, all the models were constructed using a distribution of 4 and 5 surfactant molecules on the two inside clay surfaces of the simulation box. It is remarkable then that almost symmetrical density profiles are obtained despite this initial dissymmetry.

3.2. Energetics of the Intermolecular Interactions. For the configuration of lowest potential energy determined for each system, we have also split its total potential energy into

TABLE 1: van der Waals, Electrostatic, and Total Contributions to the Binding Energies (in kcal/mol) between the Three Subsystems PCL, Surfactants, and Montmorillonite Reported for the Three Nanocomposite Systems I, II, and III

		system		
		I	II	III
$E_{\text{mnt-surf}}$	total	799	793	876
	van der Waals	271	256	341
	electrostatic	528	537	535
$E_{\text{mnt-PCL}}$	total	139	136	62
	van der Waals	86	90	42
	electrostatic	53	46	20
$E_{\text{surf-PCL}}$	total	365	372	387
	van der Waals	321	321	342
	electrostatic	44	51	45

contributions that represent only the intermolecular interactions, or more precisely, the binding energy between the three subsystems: $E_{\text{mnt-surf}}$, $E_{\text{mnt-PCL}}$, and $E_{\text{surf-PCL}}$. These represent the negative of the interaction energy between montmorillonite and the surfactant molecules, between montmorillonite and the PCL chains, and between the surfactant molecules and the PCL chains, respectively. Starting from a minimized geometry of the complete system comprising the clay platelets, the surfactants, and the chains, the calculation of the $E_{\text{mnt-PCL}}$ energy, for example, requires first the deletion of all surfactant molecules from the system. It is then obtained as the energy difference between, on one hand, the sum of the potential energy of montmorillonite and the potential energy of the chains and, on the other hand, the potential energy of the interacting montmorillonite-PCL subsystem

$$E_{\text{mnt-PCL}} = E_{\text{pot,mnt}} + E_{\text{pot,PCL}} - E_{\text{pot,mnt-PCL}}$$

Similarly, the $E_{\text{mnt-surf}}$ and $E_{\text{surf-PCL}}$ binding energies have been calculated for systems I, II, and III and are collected in Table 1 along with their respective van der Waals and electrostatic components. We first discuss the total contributions to these binding energies. Despite the difference for the interlayer densities between systems I and II, similar binding energies for the three components $E_{\text{mnt-PCL}}$, $E_{\text{mnt-surf}}$, and $E_{\text{surf-PCL}}$ are obtained. In going from system II to system III, the variations of the $E_{\text{mnt-PCL}}$ and $E_{\text{mnt-surf}}$ energies are opposite, the energy loss for $E_{\text{mnt-PCL}}$ being compensated by an energy gain for $E_{\text{mnt-surf}}$ (74 vs 83 kcal/mol). In contrast, the $E_{\text{surf-PCL}}$ energy remains nearly the same for the three systems. The relatively low $E_{\text{mnt-PCL}}$ energies calculated for the three PNC models (from 62 to 139 kcal/mol, compared to values close to 400 and 800 kcal/mol for the other two binding energies) are consistent with the prediction of Vaia et al. that systems with weak polymer-surface interactions should correspond to the intercalated structural arrangement.¹³ The evolution of the $E_{\text{mnt-PCL}}$ energetic value with respect to the density of the three systems is directly connected with the amount of polymer segments adsorbed on the clay layers. For example, the variation in the number of adsorbed segments is particularly well exemplified by comparing the geometries of systems II and III: most of the polymer segments end up in the center of the gallery for the latter system (in Figure 2c, the clay surface is mostly covered by surfactant tails) while many adsorbed segments are observed in the former (Figure 2b). Presumably, the number of adsorbed PCL segments, which decreases between system II (consisting of 3 PCL 8-mers) and system III (2 PCL 14-mers), is not resulting from the difference in the PCL chain length but is most likely related to the increase in

interlayer density. Indeed, the number of adsorbed PCL segments appears to remain approximately the same from system I to system II (as revealed by the similar $E_{\text{mnt-PCL}}$ energy values), whereas the chain length decreases from decamers to octamers. This is another result that exemplifies the discontinuities observed in the behavior of system III.

The sum of the two energy contributions where the polymer is involved, $E_{\text{surf-PCL}}$ and $E_{\text{mnt-PCL}}$, is about the same for systems I and II (~ 500 kcal/mol) and is lower by ~ 50 kcal/mol for system III. The sum of the three binding energies $E_{\text{mnt-PCL}}$, $E_{\text{mnt-surf}}$, and $E_{\text{surf-PCL}}$, which is not equivalent to the negative of the total nonbonded interaction energy since these three energies do not take into account the nonbonded interactions in a given subsystem (PCL, montmorillonite, or surfactants), amounts to 1303, 1301, and 1325 kcal/mol for systems I, II, and III, respectively. These values should not be used to evaluate the relative stability among the three systems since they represent only a fraction of the total potential energy but rather to highlight the energetic consistency between systems I and II.

The binding energies $E_{\text{surf-PCL}}$, $E_{\text{mnt-PCL}}$, and $E_{\text{mnt-surf}}$ between the various subsystems can be further separated into their van der Waals and electrostatic contributions (Table 1). In all cases, hydrophobic interactions correspond to almost 90% of the binding energy between the surfactants and the polymer chains (van der Waals term of $E_{\text{surf-PCL}}$). Large hydrophobic interactions also exist between the clay atoms and the surfactants (through mainly their hydrophobic tails) as revealed by the large van der Waals contribution (about 35% of $E_{\text{mnt-surf}}$ in all cases). Note also that both van der Waals and electrostatic energies have significant contributions to $E_{\text{mnt-PCL}}$. Therefore, if we can argue that long-range electrostatic forces could play a major role for bringing the polymer chains closer to the surface, the separation of the $E_{\text{mnt-PCL}}$ energy for the three systems is instrumental in demonstrating the importance of the van der Waals interactions between the clay and the polymer, since these constitute the dominant portion of the binding energy. This is an important conclusion from this study on polymer-charged clay interactions. A similar result has been derived by Murgich et al., but it was in the case of interactions of organic molecules with a noncharged clay platelet.⁵⁵

3.3. Conformations of the PCL Chains. For the three systems under consideration, we have also calculated the carbon-carbon radial distribution functions (RDF) for the carbon atoms of the PCL chains. This allows the study of preferential arrangements of the polymer chains inside the gallery. The profile calculated for all the polymer chains of the three systems are shown in Figure 4, along with the profile obtained for an amorphous sample of PCL consisting of 3 48-mers (this system converged toward a density of $1.04 \text{ g}\cdot\text{cm}^{-3}$, close to the value $1.09 \text{ g}\cdot\text{cm}^{-3}$ corresponding to pure amorphous PCL).⁴⁰ The peaks at ~ 1.5 and ~ 2.5 Å correspond to carbon atoms separated by one and two bonds from a reference carbon atom, respectively. The peaks at ~ 3.2 and ~ 3.9 Å correspond to pairs of carbon atoms separated by three bonds in gauche and trans conformations, respectively. For larger interatomic distances, a sharp peak exists at ~ 5.0 Å for systems I and II, while no prominent peak is visible for system III for this distance. The peak at ~ 5.0 Å arises from the occurrence of two successive trans conformations along a 5-atom-long sequence (stretched conformation comprising dihedral angles of the kinds CCCC, CCCO, or CCOC). For system III, almost the same peak heights are observed at ~ 5.0 Å (for trans-trans 1–5 pairs) and at ~ 4.5 Å (for trans-gauche 1–5 pairs). The peaks beyond

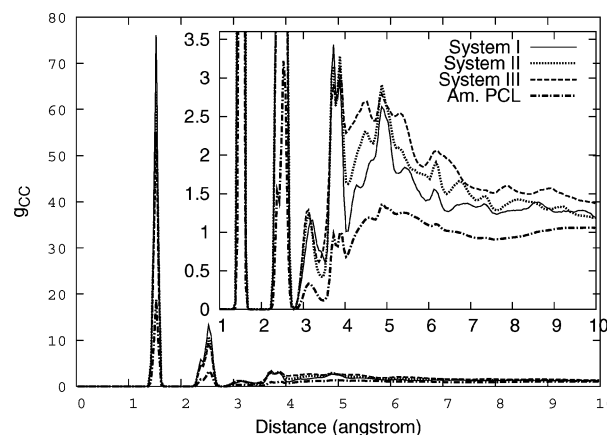


Figure 4. Radial distribution function $g_{\text{CC}}(r)$ for the carbon-carbon correlation for all PCL chains in systems I, II, and III as well as in an amorphous sample of PCL.

TABLE 2: Proportion (%) of trans Dihedral Angles for the PCL Chains and for the Surfactants Calculated for the Systems I, II, and III and for the Pure Amorphous PCL

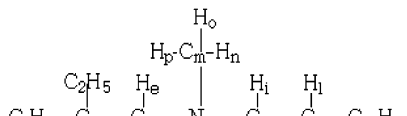
system	PCL	I	II	III
PCL chains	53	61	63	50
surfactants		54	56	51

5 Å correspond to correlations between carbon atoms separated by at least 5 bonds; they are quite small and do not provide further insight into the particular arrangements of the corresponding dihedral sequences of the polymer chains.

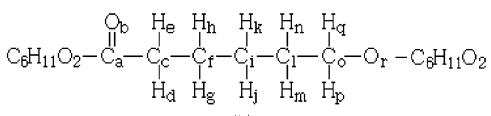
The existence of a prominent peak at 5.0 Å for systems I and II therefore indicates that many dihedral sequences along the PCL chains adopt a fully stretched conformation. The determination of the proportion of trans and gauche dihedral angles for the backbone of the chains (comprising also CCCO or CCOC dihedral types) indicates that a majority of backbone dihedrals are indeed in a trans conformation. For the three systems, the percentages of trans and gauche conformations for the backbone atoms of the PCL chains and the two aliphatic tails of all surfactants are reported in Table 2. We have also reported the corresponding percentage for the amorphous sample of PCL. It is noteworthy that the same percentages of trans conformations are obtained in systems I and II for the PCL chains on one hand (61 and 63%) and for the surfactants on the other hand (54 and 56%). In these two systems, one can also notice the higher percentage of trans angles for the polymer chains, relative to those of system III or the pure amorphous polymer sample. The proportion of trans dihedrals for system III is about the same as for the amorphous sample of PCL.

Therefore it appears that, in the two systems with lower density (I and II), the polymer chains adopt more trans conformations than in the amorphous bulk counterpart, despite the constraints they meet in the gallery. These constraints are (i) the confinement between two platelets a few tens of Å apart and (ii) the chain organization into well-defined organic layers, which both correspond to entropic penalties for the polymer chains.¹³ On the other hand, as we have seen, there are also enthalpic benefits that come from the global conformations adopted by the polymer chains, which allow interactions with both the clay surfaces (van der Waals and electrostatic interactions) and the surfactants (through mainly hydrophobic interactions) as well as a decrease in the torsional energies $\langle U_{\text{tors}} \rangle$ of the polymer chains with respect to those in amorphous bulk. In addition, the entropic penalties for the polymer chains are (at least partially) compensated by the increase in configurational freedom for the surfactant tails, as the interlayer space is

TABLE 3: Atomic Charges for (a) Selected Atoms of the Surfactant Molecule and for (b) a Caprolactone Sequence as an Example of the Typical Charges Obtained along the PCL Polymer Chains



(a)



(b)

atom index	a	b	c	d	e	f	g	h	i	j	k	l	m	n	o	p	q	r	s	t
surfactant	0.27	-0.05	-0.19	0.10	0.07	0.32	-0.25	0.11	0.12	0.07	0.01	0.00	-0.24	0.14	0.14	0.10	-0.21	0.12	0.14	0.10
PCL chain	1.04	-0.69	-0.42	0.10	0.10	0.23	-0.02	-0.02	-0.06	0.01	0.01	-0.09	0.04	0.04	0.43	-0.02	-0.02	-0.65		

enlarged in the intercalation process.^{13–15,56} The relatively low fraction of trans dihedral angles obtained for the surfactants in our results (between 51 and 56%) with respect to the much higher fractions obtained for organo-modified clay (higher than 70%) testifies to the decrease of conformational order for the surfactants after the intercalation process.^{54,57}

4. Concluding Remarks

Molecular dynamics simulations were conducted for an intercalated nanocomposite consisting of PCL chains and montmorillonite whose natural cations have been substituted with alkylammonium surfactants. To explore the influence of the amount of polymer on the molecular organization in the clay galleries, three model systems with increasing interlayer density, namely, I, II, and III, have been considered. The difference in density is brought in by modifying the length and number of polymer chains in the gallery. From a theoretical viewpoint, the consistency of models I and II indicates that the results obtained from the simulations are independent, to a certain extent, of: (i) the value of the density chosen for the organic phase; (ii) the number of polymer chains; (iii) the length of those chains. The latter two points should be taken with due caution since they are based on results obtained for models that remain of relatively modest size due to computational limitations. In contrast, the abrupt changes observed for both structural and energetic results for model III are attributable to the upper limit reached for the density of the interlayer organic phase, causing the observed discontinuities. The corresponding system should thus be regarded as modeling a limiting case.

In terms of the interactions among the components (clay, surfactant molecules, polymer chains), electrostatic interactions are of utmost importance due to the presence of the charged clay layers. Therefore, the determination of reliable charges for the polymer chains (as obtained from the *ab initio* derived electrostatic potentials and validated by simulations made for the polymer and compared with experiments) is important not only to describe the electrostatic interactions but also to enable a realistic balance between the two nonbonded potential energy terms (electrostatic and van der Waals), thus resulting in a more accurate description of the nanocomposite structure. On the basis of the predictive mean-field model of Balazs et al. for polymer nanocomposites,¹⁶ the relatively small polymer–clay binding energies obtained (with respect to the other binding energies calculated between the polymer, clay, and surfactant subsystems) are consistent with the intercalated structural arrangement observed experimentally for this material. It is important to stress that while van der Waals type interactions account for the major part of the polymer–surfactant interactions (90% of the total polymer–surfactant binding energy), the van der Waals and

electrostatic terms contribute almost equally to the polymer–clay interactions (with a slightly larger contribution from the former interaction type in the three models). From our binding energy calculations, it was found that PCL–mmt interactions account for slightly less than half (about $2/5$) of the PCL–surfactant interactions. In particular, the calculated charges have revealed the importance of hyperconjugation of the methylene group in the α position of the ester π system. This process creates an electronic deficiency on that methylene group, resulting in a large net positive charge that strongly interacts with the negatively charged clay surfaces. Thus, this hyperconjugation effect contributes to the miscibility between the PCL and the clay phases and is a driving force for the intercalation observed for this polymer; it should also be important for the intercalation of polylactide, another aliphatic polyester for which the same hyperconjugation effect exists.

The comparison between the results obtained from RDF analyses and from the dihedral angle distributions for the PCL chains in the bulk and in the intercalated nanocomposite provides evidence for a higher conformational order for the chains in the latter system. To our knowledge, the tendency toward an *increase* in conformational order has not been observed yet for a polymer/cation-exchanged clay nanocomposite by means of atomistic molecular simulations (the tendency toward an increase of stretched configurations has been observed only for models consisting of chains represented by beads interacting through a Lennard-Jones potential with confining walls).^{19,39,54,58} We conjecture that this tendency should also correspond to an increase in packing efficiency of the PCL chains inside the galleries, which may therefore explain the formation of PCL crystallites on montmorillonite surfaces, as observed experimentally for the corresponding nanocomposite.⁵⁹

Acknowledgment. The authors are grateful to Ph. Dubois, E. Pollet, M. Alexandre, and P. Brocorens (Université de Mons-Hainaut) for many fruitful discussions. Many thanks also to James Wescott (Accelrys) for providing tools for the analysis of the interlayer profiles. This project is supported by the government of the Région Wallonne, in the framework of the WDU program (TECMAVER). Research in Mons is also partly supported by the Belgian Science Policy Program (IAP Project V/3) and the Belgian National Fund for Scientific Research FNRS/FRFC.

Appendix A

For the surfactant and the oligomers, the charges were obtained with the CHELPG procedure (as implemented in the program system Gaussian 98)⁴⁷ that fits the atomic charges to the electrostatic potential calculated at the HF/6-31G* level of

TABLE 4: Valence Parameters (r_0 in Angstroms and θ_0 in Degrees) for the Element O in a PCL Chain for the Force Fields UFF and Dreiding

	UFF		Dreiding	
	r_0	θ_0	r_0	θ_0
O_R	0.680	110	0.660	120
O_2	0.634	120	0.560	120

TABLE 5: Lennard-Jones Parameters (r_0 in Angstroms and ϵ_0 in kcal/mol) for the Elements H, C, N, and O for the Force Fields UFF,³⁴ Dreiding,³⁵ and Tripos³⁶

	UFF		Dreiding		Tripos	
	r_0	ϵ_0	r_0	ϵ_0	r_0	ϵ_0
H	2.886	0.044	3.195	0.0152	3.000	0.042
C	3.851	0.105	3.8983	0.0951	3.400	0.107
N	3.660	0.069	3.6621	0.0774	3.100	0.095
O	3.500	0.060	3.4046	0.0957	3.040	0.116

TABLE 6: Distance (in Angstroms) and Energy (in kcal/mol) Parameters of the Lennard-Jones (6-12) Potential for UFF and Two Force Fields, Used in Recently Published Works, Reported for the Elements Si, Al, and O in a Clay Layer Environment

	UFF		ref 60		ref 61	
	r_0	ϵ_0	r_0	ϵ_0	r_0	ϵ_0
Si	4.295	0.402	4.700	0.400	4.550	0.040
Al	4.499	0.505	4.700	0.500	2.941	0.043
O	3.500	0.060	3.980	0.060	3.210	0.228

theory. The charges were derived for minimized geometry of the surfactant and the oligomers. The minimized conformation of the surfactant is shown in Figure 1 and was obtained from a previous RMMC exploration of its potential energy surface. For the PCL chains, an all trans minimized conformation was used for the charge calculations. The atomic charges reported for the surfactant are those around the nitrogen where the positive charge is mainly localized.

Appendix B

For the simulation of the amorphous PCL, three force fields were tested: UFF, Dreiding, and a hybrid force field that uses the Dreiding bonded parameters and the Tripos nonbonded parameters (see section 2.1). Table 4 reports the bond-stretching and angle-bending parameters for the two types of oxygen atoms in a PCL chain for UFF and Dreiding. For these two force fields, the valence parameters for C, N, and H are not shown: the respective r_0 values differ by 0.03 Å at most while the θ_0 values are all identical. The Lennard-Jones (6-12) distance (in Å) and energy (in kcal/mol) parameters of force fields UFF, Dreiding, and Tripos are reported in Table 5 for the elements H, C, N, and O.

Appendix C

In our simulations, the atoms of the clay layer are maintained in fixed positions. Thus, only nonbonded parameters for these atoms deserve attention. Table 6 reports the Lennard-Jones 6-12 parameters for UFF and for two other force fields recently used in the literature for a study of alkyl chains adsorbed on a clay surface (ref 60) and for the study of elastic properties of a montmorillonite nanoplate (ref 61).

The ϵ_0 parameters of the three force fields are the same for the three elements except for oxygen in the force field of ref 61 as its ϵ_0 parameter differs strongly with the other two parameters. The parameters r_0 in the force field of ref 60 are higher by 0.4, 0.2, and 0.5 Å than those of UFF for Si, Al, and

O, respectively. When comparing the van der Waals diameters of UFF and of the force field in ref 61, differences of ~ 0.3 Å are observed for Si and O while this parameter differs by ~ 1.6 Å for Al.

References and Notes

- (1) Alexandre, M.; Dubois, P. *Mater. Sci. Eng.* **2000**, *28*, 1.
- (2) Gloaguen, J. M.; Lefebvre, J. M. *Polymer* **2001**, *42*, 5841.
- (3) Weimer, M. W.; Chen, H.; Giannelis, E. P.; Sogah, D. Y. *J. Am. Chem. Soc.* **1999**, *121*, 1615.
- (4) Suh, D. J.; Lim, Y. T.; Park, O. O. *Polymer* **2000**, *41*, 8557.
- (5) Morgan, A. B.; Gilman, J. W.; Jackson, C. L. *Macromolecules* **2001**, *34*, 2735.
- (6) Huang, X.; Brittain, W. J. *Macromolecules* **2001**, *34*, 3255.
- (7) Zanetti, M.; Camino, G.; Thomann, R.; Mulhaupt, R. *Polymer* **2001**, *42*, 4501.
- (8) Theodorou, D. N. *Macromolecules* **1988**, *21*, 1391.
- (9) Theodorou, D. N. *Macromolecules* **1988**, *21*, 1400.
- (10) Madden, W. G. *J. Chem. Phys.* **1987**, *87*, 1405.
- (11) Bitsanis, I.; Hadziioannou, G. *J. Chem. Phys.* **1990**, *92*, 3827.
- (12) Vega, L. F.; Panagiotopoulos, A. Z.; Gubbins, K. E. *Chem. Eng. Sci.* **1994**, *49*, 2921.
- (13) Vaia, R. A.; Giannelis, E. P. *Macromolecules* **1997**, *30*, 7990.
- (14) Vaia, R. A.; Giannelis, E. P. *Macromolecules* **1997**, *30*, 8000.
- (15) Balazs, A. C.; Singh, C.; Zhulina, E. *Macromolecules* **1998**, *31*, 8370.
- (16) Balazs, A. C.; Singh, C.; Zhulina, E.; Lyatskaya, Y. *Acc. Chem. Res.* **1999**, *8*, 651.
- (17) Lee, J. Y.; Baljon, A. R. C.; Loring, R. F.; Panagiotopoulos, A. Z. *J. Chem. Phys.* **1998**, *109*, 10321.
- (18) Lee, J. Y.; Baljon, A. R. C.; Loring, R. F. *J. Chem. Phys.* **1999**, *111*, 9754.
- (19) Baljon, A. R. C.; Lee, J. Y.; Loring, R. F. *J. Chem. Phys.* **1999**, *111*, 9068.
- (20) Zax, D. B.; Yang, D. K.; Santos, R. A.; Hegemann, H.; Giannelis, E. P.; Manias, E. *J. Chem. Phys.* **2000**, *112*, 2945.
- (21) Manias, E.; Kuppa, V. *ACS Symp. Ser.* **2001**, *804*, 193.
- (22) Hackett, E.; Manias, E.; Giannelis, E. P. *Chem. Mater.* **2000**, *12*, 2161.
- (23) Kuppa, V.; Manias, E. *J. Chem. Phys.* **2003**, *118*, 3421.
- (24) Kuppa, V.; Menakanit, S.; Krishnamoorti, R.; Manias, E. *J. Polym. Sci. B: Polym. Phys.* **2003**, *41*, 3285.
- (25) Tanaka, G.; Goettler, L. A. *Polymer* **2002**, *43*, 541.
- (26) Fermeiglia, M.; Ferrone, M.; Priol, S. *Fluid Phase Equilib.* **2003**, *212*, 315.
- (27) Chávez-Páez, M.; Van Workum, K.; de Pablo, L.; de Pablo, J. J. *J. Chem. Phys.* **2001**, *114*, 1405.
- (28) Pantoustier, N.; Alexandre, M.; Degée, P.; Calberg, C.; Jérôme, R.; Henrist, C.; Cloots, R.; Rulmont, A.; Dubois, P. *e-Polymer* **2001**, *9*, 1.
- (29) Viville, P.; Lazzaroni, R.; Pollet, E.; Alexandre, M.; Dubois, P.; Borgia, G.; Pireaux, J. J. *Langmuir* **2003**, *19*, 9425.
- (30) Lepoittevin, B.; Devalckenaere, M.; Pantoustier, N.; Alexandre, M.; Kubies, D.; Calberg, C.; Jérôme, R.; Dubois, P. *Polymer* **2002**, *43*, 4017.
- (31) Lepoittevin, B.; Pantoustier, N.; Devalckenaere, M.; Alexandre, M.; Kubies, D.; Calberg, C.; Jérôme, R.; Dubois, P. *Macromolecules* **2002**, *35*, 8385.
- (32) Gaudel-Siri, A.; Brocorens, P.; Siri, D.; Gardebien, F.; Brédas, J. L.; Lazzaroni, R. *Langmuir* **2003**, *19*, 8287.
- (33) Yoon, D. Y.; Vacatello, M.; Smith, G. D. In *Monte Carlo and Molecular Dynamics Simulations in Polymer Science*; Binder, K., Ed.; Oxford University Press: New York, 1995.
- (34) Rappe, A. K.; Casewit, C. J.; Colwell, K. S.; Goddard, W. A.; Skiff, W. M. *J. Am. Chem. Soc.* **1992**, *114*, 10024.
- (35) Mayo, S. L.; Olafson, B. D.; Goddard, W. A. *J. Phys. Chem.* **1990**, *94*, 8897.
- (36) Clark, M.; Cramer, R. D., III; Opdenbosch, N. V. *J. Comput. Chem.* **1989**, *10*, 982.
- (37) Capkova, P.; Burda, J. V.; Weiss, Z.; Schenk, H. *J. Mol. Model.* **1999**, *5*, 8.
- (38) Accelrys, formerly Molecular Simulation Inc., 9685 Scranton Road, San Diego, CA, 1997.
- (39) Cui, S. T.; Cummings, P. T.; Cochran, H. D. *J. Chem. Phys.* **2001**, *114*, 6464.
- (40) Perret, R.; Skoulios, A. *Die Makromol. Chem.* **1972**, *156*, 157.
- (41) Skipper, N. T.; Chang, F. C.; Sposito, G. *Clays Clay Miner.* **1995**, *43*, 285.
- (42) Smith, D. E. *Langmuir* **1998**, *14*, 5959.
- (43) Chang, F.; Skipper, N. T.; Sposito, G. *Langmuir* **1998**, *14*, 1201.
- (44) Greathouse, J. A.; Refson, K.; Sposito, G. *J. Am. Chem. Soc.* **2000**, *122*, 11459.
- (45) Karasawa, N.; Goddard, W. A., III. *J. Phys. Chem.* **1989**, *93*, 7320.

- (46) Breneman, C. M.; Wiberg, K. B. *J. Comput. Chem.* **1990**, *11*, 361.
- (47) Frisch, M. J.; Trucks, G. W.; Schlegel, H. B.; Scuseria, G. E.; Robb, M. A.; Cheeseman, J. R.; Zakrzewski, V. G.; Montgomery, J. A., Jr.; Stratmann, R. E.; Burant, J. C.; Dapprich, S.; Millam, J. M.; Daniels, A. D.; Kudin, K. N.; Strain, M. C.; Farkas, O.; Tomasi, J.; Barone, V.; Cossi, M.; Cammi, R.; Mennucci, B.; Pomelli, C.; Adamo, C.; Clifford, S.; Ochterski, J.; Petersson, G. A.; Ayala, P. Y.; Cui, Q.; Morokuma, K.; Malick, D. K.; Rabuck, A. D.; Raghavachari, K.; Foresman, J. B.; Cioslowski, J.; Ortiz, J. V.; Stefanov, B. B.; Liu, G.; Liashenko, A.; Piskorz, P.; Komaromi, I.; Gomperts, R.; Martin, R. L.; Fox, D. J.; Keith, T.; Al-Laham, M. A.; Peng, C. Y.; Nanayakkara, A.; Gonzalez, C.; Challacombe, M.; Gill, P. M. W.; Johnson, B. G.; Chen, W.; Wong, M. W.; Andres, J. L.; Head-Gordon, M.; Replogle, E. S.; Pople, J. A. *Gaussian 98*, revision A.7; Gaussian, Inc.: Pittsburgh, PA, 1998.
- (48) Rappe, A. K.; Goddard, W. A. *J. Phys. Chem.* **1991**, *95*, 3358.
- (49) Nosé, S.; Klein, M. *Mol. Phys.* **1983**, *50*, 1055.
- (50) Nosé, S. *J. Chem. Phys.* **1984**, *81*, 511.
- (51) Hoover, W. *Phys. Rev. A* **1985**, *31*, 1695.
- (52) Dodd, L. R.; Theodorou, D. N. *Adv. Pol. Sci.* **1994**, *116*, 249.
- (53) Israelachvili, J. N. *Intermolecular and Surface Forces*; Academic Press: San Diego, CA, 1992.
- (54) Hackett, E.; Manias, E.; Giannelis, E. P. *J. Chem. Phys.* **1998**, *108*, 7410.
- (55) Murgich, J.; Rodriguez, J.; Izquierdo, A.; Carbognani, L.; Rogel, E. *Energy Fuels* **1998**, *12*, 339.
- (56) Manias, E. In *Advanced Composites*; Hyer, M. W., Loos, A. C., Ed.; Technomic Publishing Co, Inc., VA, 2001.
- (57) Venkataraman, N. V.; Vasudevan, S. *J. Phys. Chem. B* **2001**, *105*, 1805.
- (58) Cui, S. T.; Cummings, P. T.; Cochran, H. D. *J. Chem. Phys.* **2001**, *114*, 7189.
- (59) Jimenez, G.; Ogata, N.; Kawai, H.; Ogihara, T. *J. Appl. Polym. Sci.* **1997**, *64*, 2211.
- (60) Heinz, H.; Castelijns, H. J.; Suter, U. W. *J. Am. Chem. Soc.* **2003**, *125*, 9500.
- (61) Manevitch, O. L.; Rutledge, G. C. *J. Phys. Chem. B* **2004**, *108*, 1428.